CONF-781202--34

THE EFFECTS OF DELTA FERRITE CONTENT ON THE MECHANICAL PROPERTIES OF E308-16 STAINLESS STEEL WELD METAL[1]

PART III SUPPLEMENTAL STUDIES

D. P. Edmonds-Oak Ridge National Laboratory, Oak Ridge, Tennessee 37830[2]
D. M. Vandergriff-Combustion Engineering, Inc., Chattanooga, Tennessee 37402
R. J. Gray-Oak Ridge National Laboratory, Oak Ridge, Tennessee 37830[2]

ABSTRACT

The Metals Properties Council (MPC) Subcommittee I Task Group on Properties of Weldments in Elevated-Temperature Service is investigating the effects of ferrite content on the properties of type 308 stainless steel shielded metal-arc (SMA) welds. Welds were made at four levels of ferrite content ranging from 2 to 15 FN (Ferrite Number). Creep and tensile tests were performed on weld metal from each ferrite level. Also, specimens from each ferrite level were aged at 1100°C (593°C) for times up to 10,000 h (36 Ms) and Charpy V-notch impact tests were performed. This paper deals with chemical analysis of the original deposits, Magne-gage evaluations, and metallographic evaluation of tested specimens.

The E308-16 stainless steel electrodes were formulated to produce SMA welds with 2, 5, 9, and 15 FN. The ferrite number was made to vary primarily by varying the nickel and chromium concentrations. Magne-gage determinations revealed that as-welded structures contained an average of 1.8, 4.2, 9.6, and 14.5 FN, respectively. Chemical analysis of these deposits revealed no unusually high concentrations of tramp elements that would significantly affect mechanical properties. However, the extra low-ferrite electrodes were made with a different core wire, which produced deposits with slightly higher molybdenum concentrations. This variation in molybdenum content (0.25 vs 0.10% for the other deposits) should affect properties only minimally. From these chemical analyses and a constitutional diagram, ferrite concentrations were calculated, and the results correlated reasonably well with the Magne-gage values.

Aged impact specimens were evaluated after testing by Magne-gage and metallographic techniques. The measured FN decreased with increasing aging time for all welds. The decrease in measured FN resulted primarily from transformation of ferrite in the structure to sigma phase (nonmagnetic) for the welds with 10-15 FN as welded. For the lower ferrite welds the decrease in measured ferrite number resulted from transformation of ferrite to austenite and carbides. The fractures in the tested impact specimens were found in most cases to occur along inter-substructural boundaries (cellular dendritic). In general, these materials had lower impact strengths due to the presence of sigma phase and, to a lesser extent, the presence of ferrite. In the lower ferrite

[1]Metals Property Council Cooperative Program.
[2]Operated by Union Carbide Corporation, under contract W-7405-eng-26 with the U.S. Department of Energy.

welds the presence of carbides influenced the fracture propagation. Similar structures were found for the creep specimens tested at 1100°F (593°C) for times up to 10,000 h (36 Ms).

NOMENCLATURE

FN = Ferrite Number; Welding Research Council standard designation for amount of ferromagnetic phase in an austenitic stainless steel material(1).
MPC = Metal Properties Council, Inc.
QTM = Quantimet or Quantitative Television Microscope.
SMA = Shielded Metal-Arc Welding.
WRC = Welding Research Council.

INTRODUCTION

A significant problem in the production of fully austenitic stainless steel welds is their tendency for hot-cracking and microfissuring. To minimize this tendency, the compositions of welding materials are generally modified to produce small amounts of delta ferrite (usually 3 to 10 vol %) in the as-welded structure (2). However, when these materials are exposed to elevated temperatures (500 to 900°C) for extended periods of time, the ferrite can transform to a hard, brittle phase known as sigma phase (3). This transformation has been shown to lead to low-ductility creep ruptures (and to low strength in some cases) when sufficiently high stresses are applied at elevated temperatures. When this happens, ruptures occur along inter-substructural boundaries between the austenite and sigma phases (4). Concerns for the effects of varying levels of ferrite on properties of stainless steel welds exposed to elevated temperatures led to the program described in this paper.

The Metals Properties Council (MPC) Subcommittee I Task Group on Properties of Weldments in Elevated-Temperature Service is therefore investigating the effects of ferrite content on the properties of type 308 stainless steel shielded metal-arc (SMA) welds. Several companies have been involved in this study. Electrodes were formulated and manufactured at Arcos to produce welds with five respective ferrite levels. However, the welds with the highest ferrite content (19 FN) were not used in the study since they contained higher ferrite levels than would normally be expected in type 308 stainless steel weld metals. Therefore, welds with four ferrite levels ranging from 2 to 15 FN were investigated. Creep-rupture, tensile, and Charpy impact tests were performed under contract with Battelle (Columbus) on specimens from each of these four levels. Creep tests were performed at 1100°F (593°C) in air, and room-temperature impact tests were performed after aging materials in air at 1100°F (593°C) for times up to 10,000 h (36 Ms). The welds were chemically analyzed at Combustion Engineering and Arcos. Magne-gage evaluations were performed at Combustion Engineering, Arcos, and the Oak Ridge National Laboratory. Finally, selected tested creep and Charpy impact specimens were sent to the Oak Ridge National Laboratory for metallographic investigation.

CHEMICAL ANALYSES AND MAGNE-GAGE EVALUATIONS

Five lots of E308-16 electrodes were formulated to produce welds with ferrite levels ranging from 2 to 15 FN. Three types of welds were made with each lot of electrodes. First, two weld buildup pads for each lot were prepared in order to perform chemical analyses at the two testing laboratories. Multilayer pads were prepared to ensure that chemical analysis results were for weld metal with no base-metal dilution. Next, standard Welding Research Council Ferrite Pads (5) were prepared. Finally, large all-weld metal test blocks [6.25 × 6.25 × 1.25 in. (159 × 159 × 32 mm)] were prepared from each lot of electrodes.

The chemistry pads, the test blocks, and the core wires used in electrode fabrication were analyzed by spectrographic and wet chemical techniques (Table 1). Results from the two testing labs on the chemistry pads and core wires agreed very well. Therefore, only one chemical analysis was performed for the

Table 1 Chemical analyses and ferrite numbers of type 308 stainless steel weld materials

Sample	Testing[a] Lab	Chemical Composition, wt %																Ferrite Number		
		Si	S	P	Mn	C	Cr	Ni	Mo	N	Nb	Co	Cu	Al	Ti	B	V	O	AIM	Constitution Diagram[b]	Magne-Gage
Chemical Analysis Pads																					
178	C E	0.34	0.008	0.024	1.93	0.061	19.78	10.37	0.12	0.079	<0.01	0.08	0.08	<0.01	<0.01	<0.001	0.07	0.030		1.4	2.7
	Arcos	0.32	0.011	0.024	1.88	0.056	19.71	10.35	0.05	0.068									2-3	2.0	2.8
179	C E	0.33	0.008	0.024	1.67	0.060	19.97	9.28	0.11	0.085	<0.01	0.07	0.08	<0.01	<0.01	<0.001	0.07	0.028		4.7	5.4
	Arcos	0.31	0.009	0.029	1.54	1.060	19.90	9.25	0.05	0.074									5-7	5.5	6.0
180	C E	0.34	0.008	0.025	1.73	0.065	20.80	9.15	0.11	0.068	<0.01	0.07	0.07	<0.01	<0.01	<0.001	0.07	0.025		9.5	10.5
	Arcos	0.32	0.011	0.029	1.65	0.060	20.89	9.11	0.06	0.079									9-11	9.5	9.7
181	C E	0.42	0.008	0.025	1.44	0.065	20.96	8.96	0.09	0.075	<0.01	0.06	0.07	<0.01	0.01	<0.001	0.08	0.025		11.2	13.2
	Arcos	0.43	0.010	0.028	1.38	0.060	21.08	8.93	0.08	0.084									13-15	11.8	13.5
663	C E	0.32	0.012	0.034	1.69	0.062	19.18	9.98	0.14	0.067	0.01	0.05	0.06	<0.01	0.01	<0.001	0.08	0.074		1.5	0.9
	Arcos	0.32	0.009	0.030	1.62	0.067	18.92	10.15	0.25	0.097									2-3	0	0.3
Weld Metal Test Blocks																					
178	C E	0.34	0.010	0.031	1.93	0.058	20.06	10.28	0.11	0.058	0.01	0.07	0.08	<0.001	0.01	0.001	0.07	0.047	2-3	4.3	
179	C E	0.38	0.009	0.031	1.84	0.059	20.03	9.23	0.11	0.061	0.01	0.07	0.08	<0.001	0.01	<0.001	0.07	0.055	5-7	7.2	
180	C E	0.40	0.009	0.031	1.90	0.060	21.07	9.08	0.11	0.058	0.01	0.07	0.07	<0.001	0.01	0.001	0.07	0.058	9-11	12.8	
181	C E	0.47	0.009	0.032	1.55	0.062	21.34	8.94	0.10	0.062	0.01	0.07	0.07	<0.001	0.01	<0.001	0.09	0.049	13-15	14.8	
663	C E	0.37	0.009	0.027	1.60	0.060	18.90	10.42	0.25	0.053	0.01	0.05	0.06	<0.001	0.01	<0.001	0.08	0.074	2-3	1.3	
Core Wires[c]																					
Heat 2526	C E	0.47	0.010	0.022	1.72	0.046	19.91	9.38	0.12	0.044	0.01	0.08	0.08	<0.01	<0.01	0.001	0.07	0.010			
	Arcos	0.40	0.007	0.017	1.72	0.031	19.91	9.38	0.08	0.049											
Heat 3197	C E	0.45	0.010	0.025	1.60	0.054	19.47	9.29	0.25	0.048	0.01	0.04	0.07	<0.01	<0.01	0.001	0.08	0.010			
	Arcos	0.42	0.008	0.021	1.60	0.056	19.47	9.33	0.27	0.043											

[a] C E = Combustion Engineering.

[b] Source: DeLong, W. T., "Ferrite in Austenitic Stainless Steel Weld Metal," *Welding Journal (Miami)*, Vol. 53, No. 7, July 1974, pp. 273-s-286-s.

[c] Heat 2526 was used for electrode lots 178, 179, 180 and 181; heat 3197 was used for electrode lot 663.

test blocks. All weld deposits were within the specification limits for E308 weld metal, and none of the residual element concentrations were unusually high. Since electrode lot 663 was fabricated from a different core wire (Heat 3197), there was some concern that welds from this electrode would differ significantly in chemical composition. However, the only significant difference was the higher molybdenum concentrations in weld 663, which could have minor strengthening effects on the elevated-temperature properties of this material. The most significant difference between the composition of the chemistry pad and that of the corresponding test blocks is the higher nitrogen content of the chemistry pads. Finally, the primary difference between welds made with the different lots of electrodes is the chromium-to-nickel ratio, which was purposely varied to produce different ferrite levels.

The FNS for the chemistry pads and test blocks were calculated from the modified Delong Constitution Diagram (6) July 1973) using the chemical analyses in Table 1. The FN values obtained by this method (Table 1) are reasonably close to the aim ferrite levels. However, the calculated FN values for the test blocks are significantly higher — as much as 3.3 FN — than for the corresponding chemistry pads. This probably resulted from the higher nitrogen content of the chemistry pads, since nitrogen is recognized to strongly retard the formation of ferrite.

A Magne-gage was used to measure FN of the chemistry pads (Table 1), and results compare reasonably well with the values from the constitution diagram. Specimens were also removed from the test blocks, which were measured by QTM and Magne-gage (Table 2). Finally, Magne-gage determinations were performed for the Welding Research Council ferrite pads made from each of the electrodes (Table 2). The Magne-gage results from both testing labs agree very closely. Up to about 10 FN, the QTM measurements tend to exceed the corresponding Magne-gage values, but above 10 FN the trend appears to reverse itself. Additionally, the Magne-gage values for the WRC ferrite pads agree reasonably well with the constitution diagram values for the test blocks (Table 2). However, some test blocks had Magne-gage FN values significantly higher than the corresponding constitutional diagram values (for chemistry pads). In particular, the highest ferrite test blocks (181) had Magne-gage readings ranging up to 21 FN, while their constitution diagram FN value was 14.8. Therefore, the highest ferrite test blocks (181) were not included in the mechanical properties portion of this program since they contained ferrite levels higher than would normally be expected in these materials.

Mechanical properties evaluations were performed on the remaining four groups of test blocks. For ease of discussion, the blocks are referred to as extra-low-ferrite (663), low-ferrite (178), medium-ferrite (179), and high-ferrite (180) welds. No significant correlation was found between the tensile and creep properties and the measured FN in the as-welded condition. However, the room-temperature Charpy impact properties varied as a function of FN. The results of impact testing for specimens aged at 1100°F (593°C) for times ranging from 0 to 10,000 h (0 to 36 Ms) are reported in Table 3. Also included in the table are results of Magne-gage determinations on the aged specimens. Three testing laboratories measured the Magne-gage FNs of all broken impact specimens at the same location on one half of each specimen [0.375 in. (9.5 mm) from the notch on the opposite surface]. The FN values from all three labs agreed closely. The measured FN decreased with increasing aging time for all four ferrite levels (Fig. 1). Most of the decrease in FN occurred during the first 2000 h (7.2 Ms) of aging. For the unaged specimens the room-temperature impact properties decreased rapidly as the FN increased (Table 3). For instance, the average impact energy for the unaged extra-low-ferrite weld was 80.0 ft-lb (108.4 J), whereas that for the unaged high-ferrite weld was 50.2 ft-lb (68.0 J). For the extra-low- and low-ferrite welds the impact properties decreased as the FN decreased as a result of aging for times up to 2000 h (7.2 Ms). However, after further aging [5,000 and 10,000 h (18 and 36 Ms)] the impact properties leveled off and increased slightly. For the medium- and high-ferrite welds the impact properties decrease steadily as FN decreases as a result of aging. In general, there is a direct correlation between the decrease in impact properties (impact properties for the unaged specimens minus impact properties after aging) and the decrease in FN as a result of aging (Fig. 2).

Table 2 Ferrite measurements for type 308 stainless steel weld materials

Weld Block	Desired Ferrite Content (%)	QTM by BCL[a]				Magne-gage by Arcos				Magne-gage by C E[b]				Constitution Diagram (FN)	Standard[c] WRC Ferrite Pad Magne-gage, FN	
		Number of Measurements	Percent			Number of Measurements	Ferrite Number			Number of Measurements	Ferrite Number				Arcos	C E
			High	Low	Average		High	Low	Average		High	Low	Average			
178-1	2-3	50	12.4	1.0	5.2	10	2.2	1.2	1.7	8	2.05	1.35	1.67			
178-3	2-3	200	10.8	2.8	6.1	30	4.6	3.2	4.1	9	5.50	4.20	4.76	4.3	2.9	2.7
179-1	5-7	50	23.5	2.4	8.2	10	6.8	3.6	5.6	8	7.65	3.50	6.08			
179-3	5-7	200	13.0	4.0	7.6	25	10.0	8.6	9.2	9	11.05	9.10	9.67	7.2	6.7	5.4
180-2	9-11	50	17.0	3.4	10.2	10	13.4	9.8	11.52	8	12.5	9.6	11.44			
180-3	9-11	200	13.5	5.0	9.1	20	18.9	12.2	15.0	9	16.65	14.15	15.24	12.8	9.9	10.5
181-1	13-15	50	14.0	3.8	9.8	10	15.6	11.0	13.8	8	15.40	12.95	13.92			
181-3	13-15	200	15.0	6.2	9.8	30	19.7	17.5	18.6	9	20.95	17.45	18.51	14.8	13.7	13.2
663-3	1-3	200	5.6	0.8	2.4					9	2.05	0.09	1.59	1.3	0	0.3

[a] BCL: Battelle Columbus Laboratory.

[b] C E: Combustion Engineering, Inc.

[c] Source: Gunia, R. B. and Ratz, G. A., "The Measurement of Delta Ferrite in Austenitic Stainless Steels," *Welding Research Council Bulletin* No. 132, Aug. 1968.

Table 3 Magne-gage ferrite determinations of MPC E308 room-temperature Charpy V-Notch Impact Specimens after exposure at 1000°F (593°C)

Specimen	Exposure Time (h)	Impact		Lateral Expansion			Magne-Gage Ferrite Number (FN)		
		(ft-lbs)	(J)	(mils)	(mm)	(%)	C E	ARCOS	ORNL
Extra-Low-Ferrite Weld Metal									
663-3-1	0	83.0	112.5	76	1.93	19.4	0.9[a]		0.9[a]
-2	0	77.0	104.4	58	1.47	14.8	1.9		1.7
-3	0	80.0	108.5	76	1.93	19.4	1.8		1.8
Average		80.0	108.5	70	1.78	17.4	1.9		1.8
663-1-4	1,000	65.0	88.1	68	1.73	17.3	1.8		1.6
-5	1,000	66.0	89.5	60	1.52	15.3	1.7		3.0[a]
-6	1,000	71.0	96.3	68	1.72	17.3	1.5		1.8
Average		67.3	91.2	65	1.65	16.6	1.7		1.7
663-2-4	2,000	70.0	94.9	64	1.63	16.3	1.4		1.3
-5	2,000	64.0	86.8	65	1.65	16.6	1.3		1.1
-6	2,000	65.5	88.8	70	1.78	17.4	1.0		1.0
Average		66.5	90.1	66	1.68	16.8	1.2		1.1
663-2-1	5,000	83	112.5	88	2.24	22.4	0.3		0.2
-2	5,000	86	116.6	83	2.11	21.2	0.3		0.2
-3	5,000	86	116.6	86	2.18	21.9	0.4		0.2
Average		85	115.2	86	2.18	21.8	0.3		0.2
663-1-1	10,000	85.5	115.9	86	2.18	21.9	0.3		0.2
-2	10,000	85.5	115.9	86	2.18	21.9	0.3		0.2
-3	10,000	78.5	106.4	76	1.93	19.4	0.3		0.2
Average		83.2	112.8	83	2.11	21.1	0.3		0.2
Low-Ferrite Weld Metal									
178-3-7	0	62.0	84.1	61	1.55	15.4	4.2	3.8	4.1
-8	0	59.0	80.0	61	1.55	15.5	4.1	3.5	3.9
-9	0	70.0	94.9	70	1.78	17.7	5.1	4.5	4.9
Average		63.7	86.4	64	1.63	16.2	4.5	3.9	4.3
178-2-10	1,000	55.5	75.2	63	1.60	15.9	2.6	2.2	2.4
-11	1,000	55.0	74.6	60	1.52	15.2	2.6	2.2	2.3
-12	1,000	51.5	69.8	57	1.45	14.4	2.6	2.2	2.4
Average		54.0	73.2	60	1.52	15.2	2.6	2.2	2.4
178-2-7	2,000	47.0	63.7	57	1.47	14.6	2.1	1.6	2.0
-8	2,000	46.0	62.4	52	1.32	13.1	2.2	1.9	2.1
-9	2,000	42.5	57.6	50	1.27	12.6	2.1	1.6	1.8
Average		45.2	61.3	53	1.35	13.4	2.1	1.7	2.0
178-2-4	5,000	51.0	69.1	69	1.75	17.4	1.9	1.4	1.9
-5	5,000	51.5	69.8	58	1.47	14.7	2.1	1.4	2.1
-6	5,000	57.0	77.3	66	1.68	16.7	1.3	1.4	1.7
Average		53.2	72.1	64	1.62	16.3	1.8	1.4	2.1
178-2-1	10,000	49.0	66.4	51	1.29	13.0	1.5	1.4	1.2
-2	10,000	44.0	59.7	44	1.11	11.2	1.7	1.4	1.7
-3	10,000	55.0	74.6	50	1.27	12.7	1.3	0.8	1.5
Average		49.3	66.8	48	1.22	12.3	1.5	1.2	1.5
Medium-Ferrite Weld Metal									
179-3-7	0	52.0	70.5	54	1.37	13.7	10.2	9.7	10.1
-8	0	52.5	71.2	53	1.34	13.4	9.7	9.0	9.3
-9	0	54.0	73.2	57	1.45	14.4	8.7	10.0	8.4
Average		52.8	71.6	55	1.40	13.8	9.5	9.6	9.3
179-2-10	1,000	45.0	61.0	49	1.24	12.4	6.1	5.3	5.5
-11	1,000	36.5	49.5	42	1.06	10.6	5.8	5.3	5.5
-12	1,000	35.0	47.5	38	0.96	9.6	4.4	4.0	4.2
Average		38.8	52.6	43	1.09	10.9	5.4	4.9	5.1
179-2-7	2,000	39.0	52.9	44	1.12	11.1	4.7	4.2	4.3
-8	2,000	32.0	43.4	43	1.10	10.9	5.3	4.0	4.6
-9	2,000	27.5	37.3	36	0.91	9.1	4.0	4.5	4.7
Average		32.8	44.5	41	1.04	10.4	4.7	4.2	4.4
179-2-4	5,000	18.0	24.4	24	0.61	6.2	4.2	3.8	4.1
-5	5,000	19.5	26.4	27	0.69	6.8	4.1	3.8	4.0
-6	5,000	21.5	29.2	25	0.64	6.3	3.7	3.8	3.5
Average		19.7	26.7	25	0.64	6.4	4.0	3.8	3.9
179-2-1	10,000	18.0	24.4	19	0.48	4.8	3.5	3.2	3.4
-2	10,000	19.0	25.8	23	0.58	5.8	2.4	3.0	3.3
-3	10,000	19.5	26.4	18	0.46	4.6	2.3	2.7	3.2
Average		18.8	25.5	20	0.51	5.1	2.7	3.0	3.3
High-Ferrite Weld Metal									
180-3-7	0	46.0	62.4	43	1.09	10.9	15.9	14.9	15.8
-8	0	53.0	71.9	59	1.50	14.9	12.9	11.9	12.4
-9	0	51.5	69.8	61	1.55	15.4	16.7	14.6	16.1
Average		50.2	68.1	54	1.37	13.7	15.2	13.8	14.8
180-2-10	1,000	14.5	19.7	18	0.46	4.6	6.9	6.1	6.7
-11	1,000	20.5	27.8	21	0.53	5.3	6.7	6.1	6.4
-12	1,000	18.5	25.1	21	0.53	5.3	7.4	6.6	6.7
Average		17.8	24.1	20	0.51	5.1	7.0	6.3	6.6
180-2-7	2,000	13.5	18.3	14	0.36	3.5	5.4	5.0	5.5
-8	2,000	13.5	18.3	14	0.36	3.5	5.4	4.8	5.4
-9	2,000	13.5	18.3	14	0.36	3.5	5.8	5.3	5.6
Average		13.5	18.3	14	0.36	3.5	5.5	5.0	5.5
180-2-4	5,000	13.0	17.6	13	0.33	3.3	4.1	3.5	3.9
-5	5,000	11.5	15.6	12	0.30	3.0	3.6	3.2	3.6
-6	5,000	12.0	16.3	12	0.30	3.0	3.6	3.2	3.5
Average		12.5	17.0	12	0.30	3.1	3.8	3.3	3.7
180-2-1	10,000	11.5	15.6	11	0.28	2.8	3.1	3.0	3.1
-2	10,000	14.0	19.0	16	0.41	4.1	3.2	2.7	3.0
-3	10,000	12.5	17.0	11	0.28	2.8	3.1	2.4	3.0
Average		12.7	17.2	13	0.33	3.3	3.1	2.7	3.0

[a]Data point not included in average.

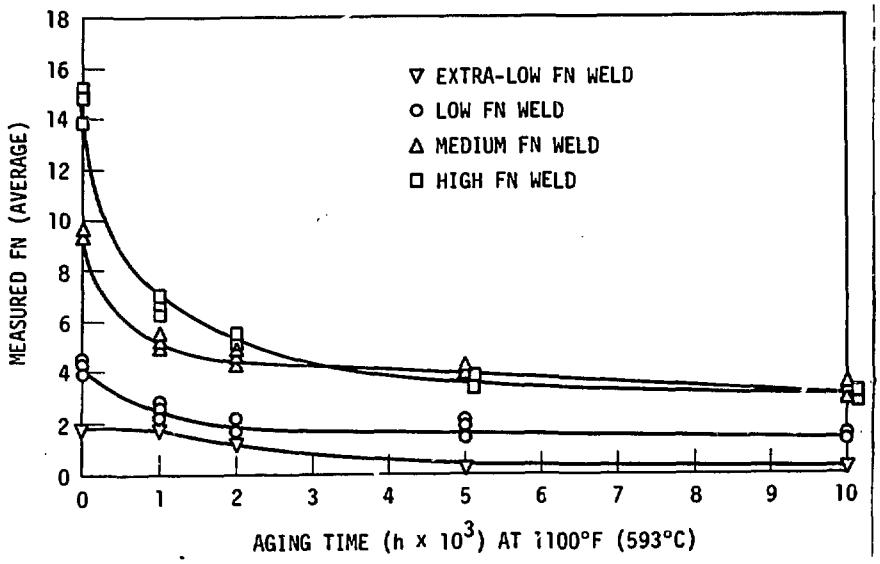

Fig. 1 Decrease in average measured FN after aging at 1100°F (593°C).

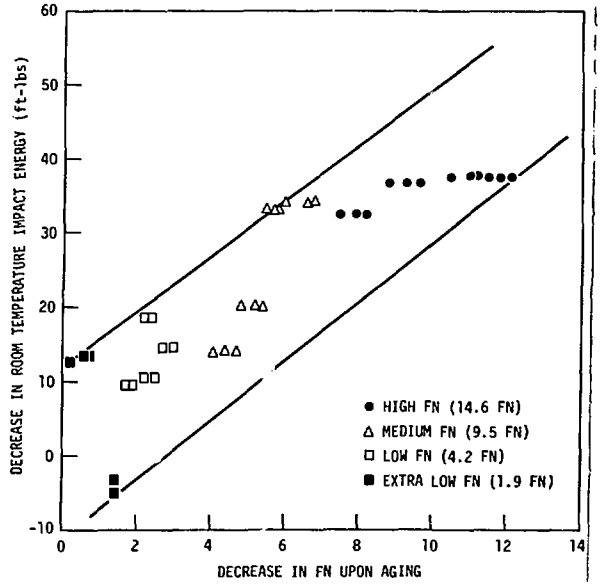

Fig. 2 Decrease in Charpy impact strength as a function of decrease in FN upon aging at 1100°F (593°C).

METALLOGRAPHIC EVALUATION

In an attempt to explain changes observed in mechanical properties and measured ferrite number (FN), tested specimens were metallographically evaluated. Selected creep and impact specimens from the four ferrite levels were examined. Optical metallographic evaluations of the specimens were performed with color and magnetic colloid etching techniques. With the color etching technique, austenitic, ferritic, and sigma phases can be distinguished optically. Each specimen is preheated and immersed in an alkaline potassium ferricyanide solution etchant [30 g KOH, 30 g $K_3Fe(CN)_6$, 100 ml H_2O] at 203°F (95°C) for 8 s. From this treatment sigma phase turns brownish red, ferrite turns dark gray, austenite remains light gray, and carbides turn black. The magnetic colloid etchant (7,8) is used to determined microscopic patterns of ferromagnetic phases in a structure. With this technique a ferrofluid — a colloidal dispersion of fine iron in an organic or aqueous fluid — is placed between the polished and etched specimen surface and a thin glass slide. The assembly is then placed on a metallograph and is surrounded by a direct-current electromagnet (coil). When the coil is energized, the iron particles are attracted to ferromagnetic constituents — ferrite and martensite — in the microstructure. Since the specimens have already been etched by conventional techniques, the ferromagnetic characteristics of microscopic constituents can be defined. With this technique, delta ferrite and strain-induced martensite have been detected and identified in austenitic stainless steel materials (7,8).

General microstructures of the low-, medium-, and high-ferrite welds are shown in Figs. 3, 4, and 5, respectively. Microstructures after aging for 5000 and 10,000 h (18 and 36 Ms) at 1100°F (593°C) are also shown in these figures. Since these figures are black and white, austenite is very light gray, ferrite is slightly darker gray, and sigma and carbides are black. The unaged microstructures consisted of ferrite and carbides in austenitic matrices. Strain-induced martensite was not found in any of these specimens. However, martensite in austenitic stainless steels is sometimes very difficult to detect

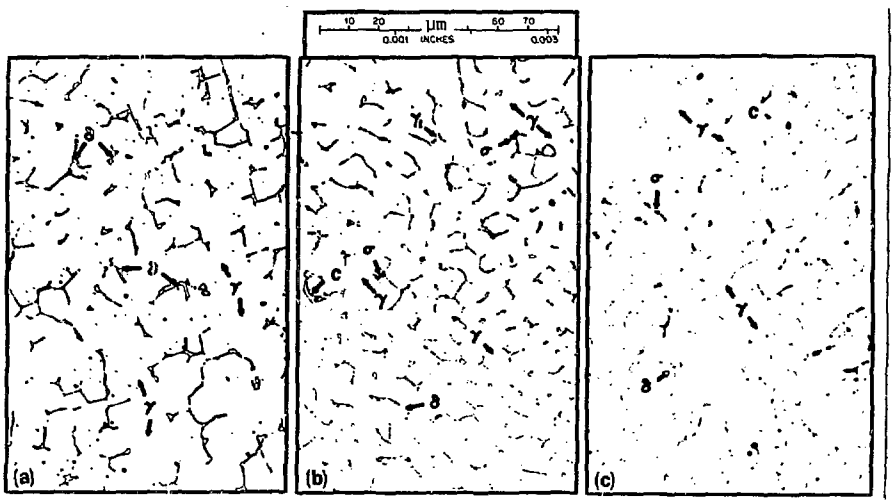

Fig. 3 Micrographs showing the predominance of ferrite-to-austenite phase transformation in low-ferrite E308 stainless steel welds exposed at 1100°F (593°C) in air. Phases: austenite — γ; ferrite — δ; transformed austenite — γ_t; carbide — C; sigma — σ. (a) As welded: 4.0 FN. (b) Exposed 5000 h: 1.9 FN. (c) Exposed 10,000 h: 1.4 FN.

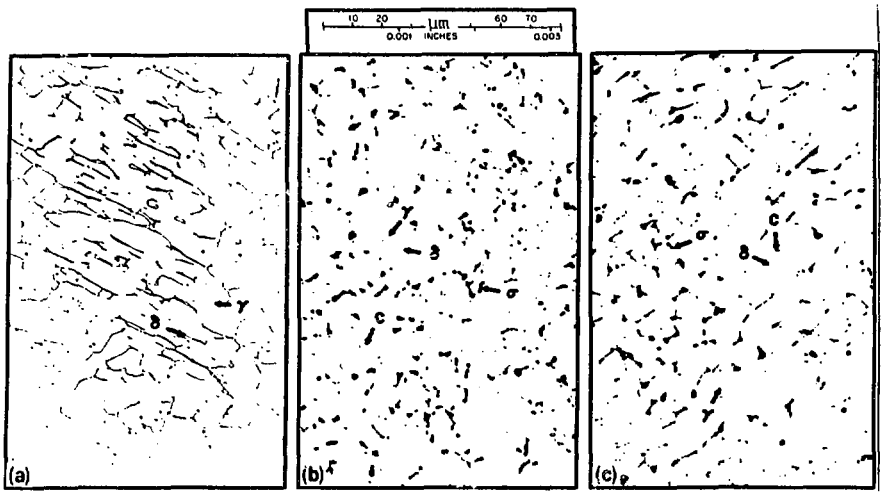

Fig. 4 Micrographs showing the predominance of ferrite-to-sigma phase transformation in medium-ferrite E308 stainless steel welds at 1100°F (593°C) in air. Phases: austenite — γ; ferrite — δ; carbide — C; sigma — σ. (a) As welded: 9.3 FN. (b) Exposed 5000 h: 4.0 FN. (c) Exposed 10,000 h: 2.9 FN.

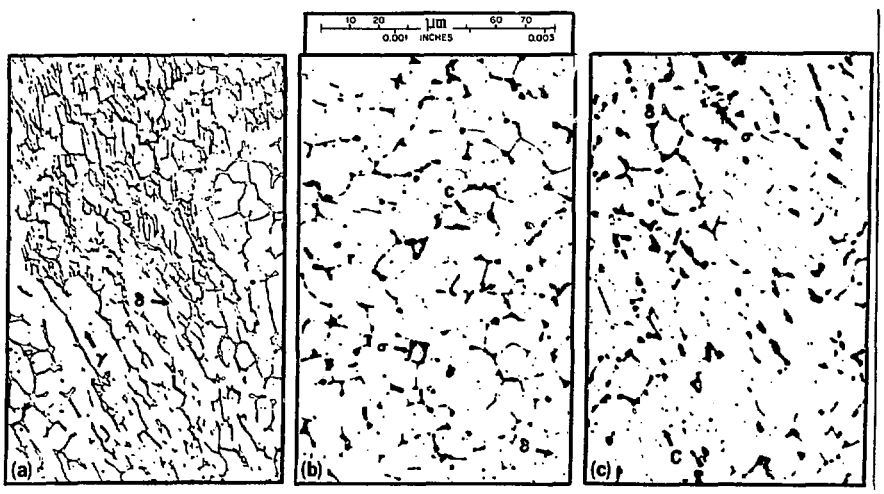

Fig. 5 Micrographs showing the ferrite-to-sigma phase transformation to predominate in high-ferrite E308 stainless steel welds exposed at 1100°F (593°C) in air. Phases: austenite — γ; ferrite — δ; carbide — C; sigma — σ. (a) As welded: 15.8 FN. (b) Exposed 5000 h: 3.4 FN. (c) Exposed 10,000 h: 2.8 FN.

and may be masked by the other constituents. Finally, in the unaged materials, the ferrite islands become continuous at about 10 FN (Fig. 4).

Aging at 1100°F (593°C) had different effects on the microstructure of the extra-low- and low-ferrite welds than on the medium- and high-ferrite welds. For the medium- and high-ferrite welds (Figs. 4 and 5) the measured decrease in FN upon aging resulted primarily from the transformation of ferrite to sigma phase. However, in the low- (Fig. 3) and extra-low-ferrite welds little of the ferrite phase transformed to sigma. Most of the ferrite formed carbides — probably chromium carbides — which nucleated and grew at the ferrite-austenite boundary, leaving the ferritic phase deficient in chromium. This is believed to allow some of the ferrite phase to transform to austenite [Fig. 3(c)] and thus, decrease the measured FN. These transformed areas were not the characteristic brownish-red color of sigma phase, nor was there a visible boundary between these areas and the austenite matrix.

An extra-low-ferrite weld was examined with the magnetic colloid technique to confirm that the above transformation was indeed to austenite (Fig. 6). Several of the ferrite islands that typically show a ferromagnetic response (black hazy areas) were no longer ferromagnetic after aging [Fig. 6(b)] for 5000 h (18 Ms). Note that the number of areas that attract the ferrofluid is larger in Fig. 6(a) than in Fig. 6(b). However, the amount of ferrofluid attracted to each area is greater in Fig. 6(b). This does not mean, however, that the ferromagnetic response or the size of these areas is greater for the aged materials [(Fig. 6(b)]. This effect results from the fact that for a given amount of ferrofluid on each specimen surface, more ferrofluid is available for each ferromagnetic area when fewer auch areas are present. This technique detected no martensite in the structure. Carbide precipitates also transformed to austenite in the medium- and high-ferrite welds, but not as much as in the lower ferrite welds.

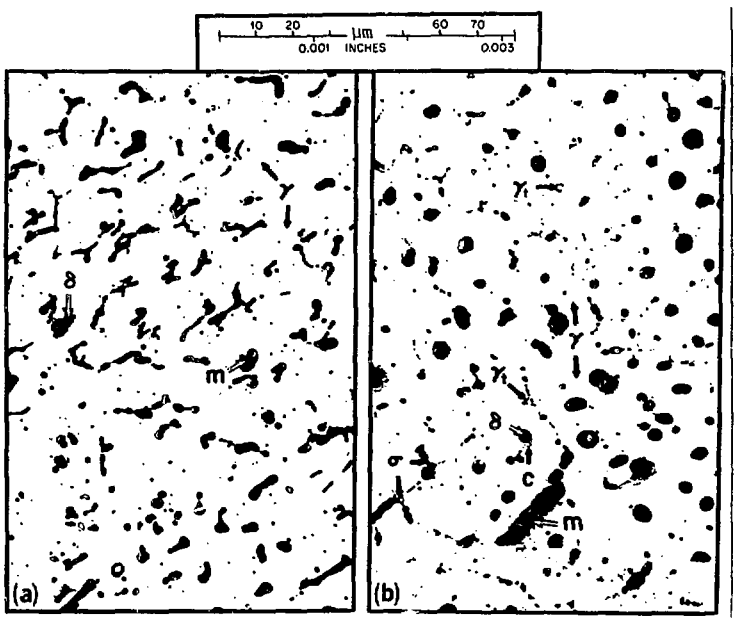

Fig. 6 Ferrite-to-austenite phase transformation as detected by magnetic colloid etching in extra-low-ferrite E308 stainless steel welds. Key: austenite — γ; ferrite — δ; carbide — C; sigma — σ; magnetic colloid — M; transformed austenite — γ_t. (a) As welded: 1.8 FN. (b) Exposed 5000 h: 0.3 FN.

In all specimens, some ferrite was still present after aging for 10,000 h (36 Ms). The transformation to sigma phase in the high- and medium-ferrite weld began very quickly: it was observed after only 8 h (.03 Ms) in one of the creep specimens (Fig. 7). Small stringers of ferrite transformed to carbides, austenite, or sigma phase more readily than did the larger islands of ferrite. When the ferrite islands transformed to sigma phase, they most often became more agglomerated and appeared to consume some of the austenite in the transformation [Fig. 5(c)].

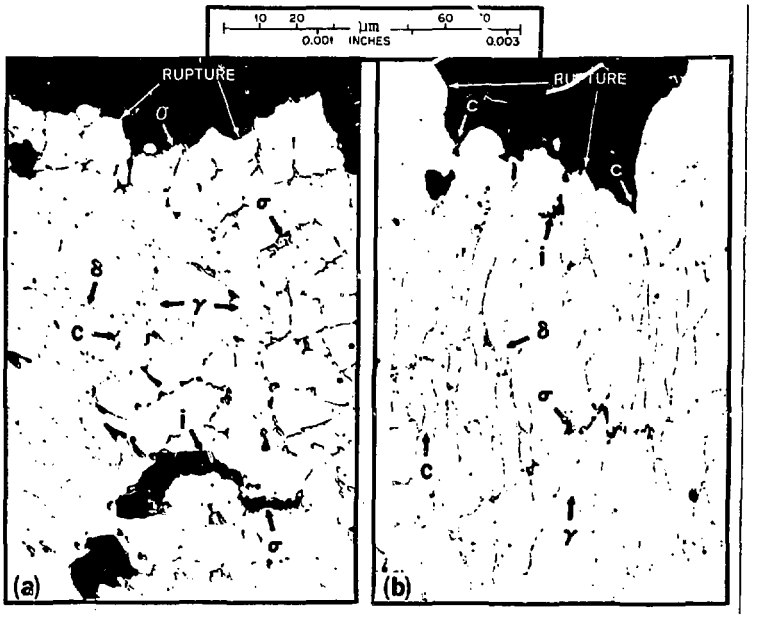

Fig. 7 Creep ruptures associated with transformed sigma phase in high-ferrite E308 stainless steel welds tested at 1100°F (593°C) in air. Key: austenite — γ; ferrite — δ; interphase separation — i; carbide — C; sigma — σ. (a) Weld exposed to 24.0-ksi (16.5-MPa) stress until rupture at 7562.6 h; total elongation — 3.4%. (b) Weld exposed to 45.0-ksi (310-MPa) stress until rupture at 7.6 h; total elongation — 30.2%.

Micrographs transverse to the fracture surface of the low- and high-ferrite impact specimens are shown in Figs. 8 and 9. Fracture profiles for the extra-low-ferrite welds resembled those shown in Figs. 8 and the medium-ferrite welds resembled those in Fig. 9. For all unaged specimens, the fractures did not appear to relate directly to the substructure. Also, no secondary cracks were found in any of the unaged specimens. However, the substructure significantly affected the fractures in the aged specimens. In the aged low- and extra-low-ferrite welds, fractures appeared to propagate more readily along carbide-austenite boundaries (Fig. 3). In the aged medium- and high-ferrite welds, fractures propagated more readily along the austenite-sigma phase boundaries (Fig. 9). Secondary cracks were found in all aged specimens.

Similar results were found for the ruptured creep specimens (Figs. 7 and 10) tested at 1100°F (593°C). Ruptures in the lower ferrite welds were associated with carbide formation, while those in the higher ferrite welds were associated with transformation to sigma phase. A classic creep void forming along austenite-sigma phase boundaries in a medium-ferrite weld [tested for 7800 h (28 Ms) at 1100°F (593°C)] is shown in Fig. 11.

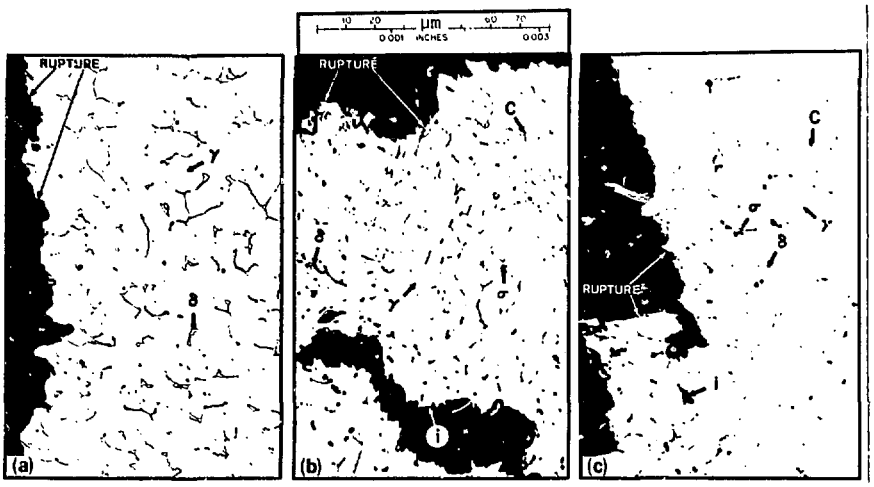

Fig. 8 Charpy fracture profiles associated with precipitated carbides for the low-ferrite E308 stainless steel weld exposed at 1100°F (593°C) in air. Key: austenite — γ; ferrite — δ; interphase separation — i; carbide — C; sigma — σ. (a) As welded: 4.0 FN. (b) Exposed 5000 h: 1.9 FN. (c) Exposed 10,000 h: 1.4 FN.

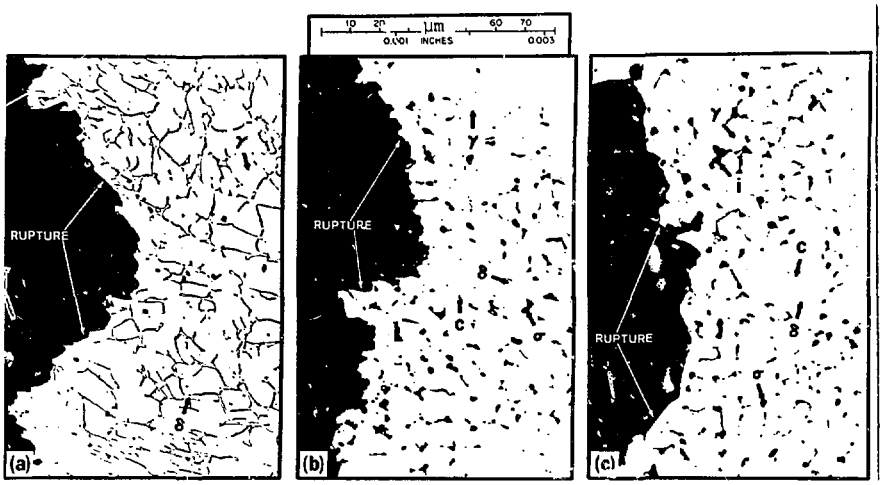

Fig. 9 Charpy fracture profiles associated with transformed sigma phase in high-ferrite E308 stainless steel welds exposed at 1100°F (593°C) in air. Key: austenite — γ; ferrite — δ; interphase separation — i; carbide — C; sigma — σ. (a) As welded: 15.8 FN. (b) Exposed 5000 h: 3.4 FN. (c) Exposed 10,000 h: 2.8 FN.

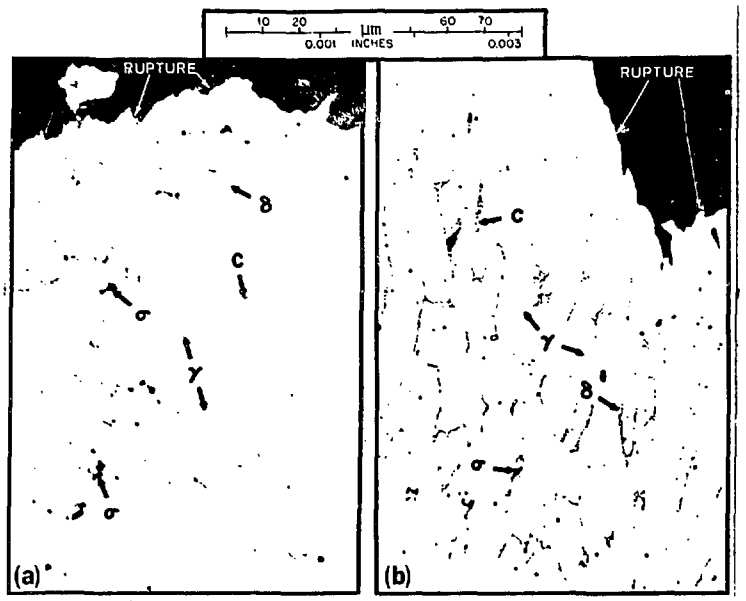

Fig. 10 Creep ruptures associated with precipitated carbides in the extra-low-ferrite E308 stainless steel welds tested at 1100°F (593°C) in air. Key: austenite — γ; ferrite — δ; carbide — C; sigma — σ. (a) Weld placed under 30.5-ksi (210 MPa) stress until rupture at 4961.0 h; total elongation — 3.4%. (b) Weld placed under 45.0-ksi (310-MPa) stress until rupture at 10.7 h; total elongation — 28.5%.

Therefore, two mechanisms appear to operate in these welds upon exposure to elevated temperatures. For the lower ferrite welds, the transformation of ferrite to carbides and austenite has the greater effect on properties, while for the higher ferrite welds, transformation of ferrite to sigma has the greater effect. We feel that differences between these transformations cause Charpy impact properties to differ. That is, the higher impact properties for the aged lower ferrite welds resulted from the transformation of ferrite to austenite and the formation of carbides, while the lower properties for the aged higher ferrite welds resulted from sigma phase formation. As the previous section indicated, creep properties at 1100°F (593°C) did not correlate significantly with FN (as welded). Therefore, both transformations — to carbides and to sigma phase — appear equally detrimental to creep properties, while the sigma phase transformation is much more detrimental than carbide formation to the Charpy impact properties. We should again point out that both transformations occur to some extent in all exposed specimens, but that the above transformation predominated for the materials in this study.

The exact reason for these transformations is not clear. However, the ferrite that formed in the lower ferrite welds may have contained less chromium than the ferrite in the higher ferrite welds. Lower chromium ferrite may transform more readily to carbides and austenite, while higher chromium ferrite may transform more readily to sigma phase. This postulation has not, however, been proven here and is not within the scope of this study.

CONCLUSIONS

1. Differences between the chemical composition of the small chemistry pads and that of the larger test blocks were large enough to produce significantly higher calculated FN values for the test blocks (greater than 3 FN in

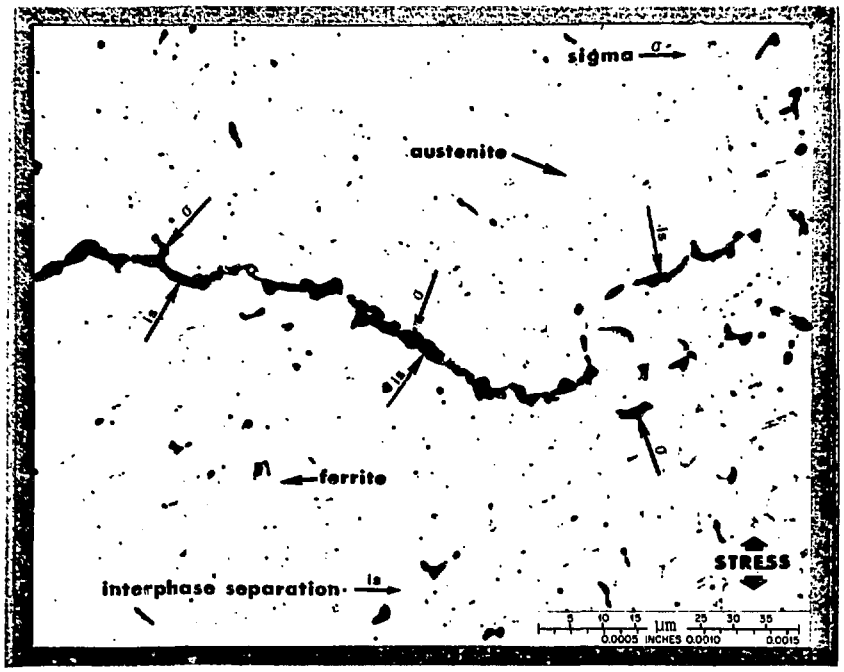

Fig. 11 Interphase separation between austenite and sigma phases in medium-ferrite E308 stainless steel weld, as revealed by color etching. Rupture life — 7797 h; total elongation — 4.1%; test temperature — 1100°F (593°C); stress — 25.5 ksi (175.8 MPa).

some cases). The higher FN probably resulted from the higher nitrogen concentrations in the test blocks, which resulted from differences in welding conditions for the two types of weld.

2. The measured FN of the test blocks was also significantly higher than that of the corresponding WRC ferrite pad for the same reason as above.

3. The results of chemical analyses from two testing labs and the Magnegage results from three labs agreed closely.

4. Tensile and creep properties did not correlate significantly with measured FN (as-welded condition) of these materials.

5. The measured FN decreased with increasing exposure time at 1100°F (593°C), with most of the decrease occurring in the first 2000 h (7.2 Ms).

6. Room-temperature Charpy impact properties decreased rapidly as FN in the unaged specimens increased.

7. In general, decreases in room-temperature Charpy impact properties correlate directly with decreases in measured FN as a result of exposure at 1100°F (593°C).

8. In the as-welded structures, ferrite morphology became continuous at a level of approximately 10 FN.

9. Decreases in measured FN with aging at 1100°F (593°C) resulted primarily from the transformation of ferrite to sigma phase for the higher ferrite welds, and of ferrite to austenite and carbides for the lower ferrite welds. Both transformations occurred in all ferrite levels of this material.

10. Morphology changes occur with the transformation of ferrite to sigma. The sigma islands become more agglomerated than the original ferrite, and some of the surrounding austenite is apparently consumed in the transformation.

11. For all specimens in the as-welded conditions, Charpy impact fractures did not appear to relate directly to the substructure.

12. In specimens aged at 1100°F (593°C), Charpy impact fractures propagated along austenite-sigma phase boundaries for the higher ferrite welds, while fractures were associated with carbides in the lower ferrite welds.

13. Secondary cracks were not found in unaged Charpy impact specimens, but were found in all aged specimens that we investigated.

14. The investigation of ruptured creep specimens gave similar results. That is, the ruptures propagated along austenite-sigma phase boundaries in the higher ferrite welds but were associated with carbides in the lower ferrite welds.

15. The transformation of ferrite to sigma phase (higher ferrite welds) is much more detrimental to room-temperature Charpy impact properties than carbide formation (lower ferrite welds), while both transformations are equally detrimental to creep properties.

ACKNOWLEDGMENTS

The authors acknowledge the technical guidance provided by the Metals Properties Council Task Force on the Properties of Weld Metals of Subcommittee I, chaired by W. D. Doty, and in particular, the Working Group on Metallographic and Magne-gage Determination. Members of this working group include G. S. Sangdahl, G. M. Slaughter, R. D. Thomas, D. M. Vandergriff, and D. P. Edmonds. Also, technical assistance was provided by G. M. Goodwin and J. M. Leitnaker. Thanks are also extended to Nan Richards for editing, and to Connie Harrison for typing the manuscript. The research was sponsored jointly by the U.S. DOE, Combustion Engineering, Inc., and Arcos Corporation.

REFERENCES

1 American Welding Society Specification A4.2-74, "Standard Procedures for Calibrating Magnetic Instruments to Measure the Delta Ferrite Content of Austenitic Stainless Steel Welding Metal."

2 Borland, J. C. and Younger, R. N., *Some Aspects of Cracking in Welded Chromium-Nickel Austenitic Steels,* BWRA Report B5/1/59 Aug. 1959, British Welding Research Association, London, England.

3 Malone, M. O., "Sigma and 885°F Embrittlement of Chromium-Nickel Stainless Steel Weld Metals," *Welding Journal, (New York),* Vol. 46, No. 6, June 1967, pp. 241-s-253-s.

4 Binkley, N. C., Goodwin, G. M., and Harman, D. G., "Effects of Electrode Coverings on Elevated Temperature Properties of Austenitic Stainless Steel Weld Metal," *Welding Journal (Miami),* Vol. 52, No. 7, July 1973, pp. 306-s-311-s.

5 Guina, R. B. and Ratz, G. A., "The Measurement of Delta Ferrite in Austenitic Stainless Steels," *Welding Research Council Bulletin* No. 132, August 1968.

6 DeLong, W. T., "Ferrite in Austenitic Stainless Steel Weld Metal," *Welding Journal (Miami),* Vol. 53, No. 7, July 1974, pp. 273-s-286-s.

7 Gray, R. J., "Magnetic Etching with Ferrofluid," *Metallographic Specimen Preparation,* Plenum Publishing Company, New York, 1973.

8 Gray, R. J., "The Detection of Strain-Induced Martensite in Types 301 and 304 Stainless Steels by Epitaxial Ferromagnetic Etching," *Microstructural Science,* Vol. 1, American Elsevier Publishing Company, Inc., New York, 1972, pp. 159-175.